Effect of Different Amount of Conductive Carbon Material Content on the Electrochemical Performance of LiFePO4 Cathode for Li-ion Batteries

Debabrata Mohanty , Min-Jie Chang , I-Ming Hung *

Posted Date: 22 September 2023

doi: 10.20944/preprints202309.1494.v1

Keywords: LiFePO4 cathode; Super P; Conductive carbon; Electrochemical property; Li+ ion diffusion coefficient

Article

Effect of Different Amount of Conductive Carbon Material Content on the Electrochemical Performance of $LiFePO_4$ Cathode for Li-ion Batteries

Debabrata Mohanty [1], Min-Jie Chang [1] and I-Ming Hung [1,2,*]

[1] Department of Chemical Engineering and Materials Science, Yuan Ze University, 135 Yuan-Tung Road, Chung-Li, Taiwan 32003, Taiwan; debabratamohanty1997@gmail.com (D. Mohanty); tracy881017@gmail.com (M-J. Chang); imhung@saturn.yzu.edu.tw (I-M. Hung)

[2] Hierarchical Green-Energy Materials (Hi-GEM) Research Center, National Cheng Kung University, Tainan 70101, Taiwan; imhung@saturn.yzu.edu.tw (I-M. Hung)

* Correspondence: imhung@saturn.yzu.edu.tw; Tel.: +886-3 -463-8800

Abstract: $LiFePO_4$ (LFP) has undergone extensive research and is a promising cathode material for Li-ion batteries. The high interest is due to its low raw material cost, good electrochemical stability, and high-capacity retention. However, poor electronic conductivity and a low Li^+ diffusion rate decrease its electrochemical reactivity, especially at fast charge/discharge rates. In this work, the volumetric energy density of lithium-ion batteries is successfully increased by using different amounts of conductive carbon (Super P) in the active material content. The particle size and morphology of the electrode material samples are studied using field emission scanning electron microscopy and dynamic light scattering. Two-point-probe DC measurements and adhesive force tests are used to determine the conductivity and evaluate adhesion for the positive electrode. Cyclic voltammetry, electrochemical impedance spectroscopy (EIS), and charge/discharge tests are used to analyze the electrochemical properties of the battery. The samples containing 88% LFP, 5.5% Super P and 6.5% PVDF perform best, with discharge capacities reaching 169.8 $mAhg^{-1}$ at 0.1C, and they can also manage charging/discharging of 5C. EIS indicates that this combination produces the lowest charge-transfer impedance (67 Ω) and the highest Li^+ ion diffusion coefficient (5.76 x 10^{-14} cm^2s^{-1}).

Keywords: $LiFePO_4$ cathode; Super P; conductive carbon; electrochemical property; Li^+ ion diffusion coefficient

1. Introduction

In-depth research has recently focused on the large-scale application of Li-ion batteries in hybrid electric vehicles (HEVs) and backup power systems. Although $LiCoO_2$ is already successfully commercialized in small lithium-ion batteries, using it as the cathode material in large-scale lithium-ion batteries is still challenging due to safety problems and high cost [1, 2]. Thanks to its relatively low cost and safer operation, $LiFePO_4$ is considered an ideal material to utilize as the cathode in large-scale lithium-ion batteries [3, 4]. Additional benefits of $LiFePO_4$-based batteries for powering electric vehicles (EVs) and plug-in hybrid electric vehicles (PHEVs) are their high theoretical capacity (170 $mAhg^{-1}$), high tolerable voltage (3.5 V), superior cycle performance, excellent thermal stability, environmental friendliness, low self-discharge, and safety of olivine-type $LiFePO_4$ [5-8]. For two decades, $LiFePO_4$ has been the subject of extensive research in both scientific and engineering applications [9]. Despite the numerous benefits, $LiFePO_4$ in LIBs still faces challenges, particularly because of the suboptimal low-temperature electrochemical performance in transportation applications [10, 11]. The low electrical conductivity of $LiFePO_4$ (around 10^{-9} to 10^{-10} S cm^{-1} at room temperature) and the slow lithium-ion diffusivity (around 10^{-14} to 10^{-16} cm^2 s^{-1} at room temperature) are the main reasons for the relatively poor low-temperature electrochemical performance. This is contrary to earlier reports that claimed the choice of the cathode material mainly determines the low-temperature electrochemical performance [12, 13].

Shin et al. discovered in 2013 that pure $LiFePO_4$ improves cycle stability at lower operating temperatures (20 °C) [14]. It was also found that bulk- and surface- deterioration was significantly reduced for low temperatures. In addition, significant efforts were made to improve the low-temperature electrochemical performance of the $LiFePO_4$ cathode, which includes the following: (i) coating the surface of $LiFePO_4$ with carbon or other conducting materials to increase the electronic conductivity [15], (ii) reducing the particle size to shorten diffusion distances and increase surface area [16], and (iii) doping with super-valent cations or metal oxides to improve intrinsic electronic conductivity [17]. Moreover, both the surface reaction kinetics and the rate of charge (for lithium-ions and electrons) diffusion inside the electrode bulk slow down with decreasing operating temperature [18, 19]. Consequently, the electrode faces a greater challenge under such conditions.

Generally, carbon coating is considered highly efficient as it hinders particle growth during sintering, leading to reduced particle size. Additionally, it enhances the electronic conductivity of the active particles' surface [20-22]. This method is widely used and extensively studied. In other words, the combination of smaller particle size and carbon coating should significantly enhance the electrochemical performance of $LiFePO_4$ [23]. $LiFePO_4$ materials with carbon coatings were successfully created by Zhao et al. in 2016 using polystyrene spheres (50-300 nm) as the carbon source [24]. The results showed that $LiFePO_4$/C, which contains 3.0 weight percent carbon, performed electrochemically well at 20 °C, delivering 147 $mAhg^{-1}$ and 79.3 $mAhg^{-1}$ at 0.1 C and 1 C. Moreover, $LiFePO_4$/C showed approximately 100% capacity retention – even after 100 cycles at 1 C. This is due to the ideal thickness (2.5 nm) and suitable shape of the carbon coating [25]. As an alternative, Yang et al. studied $LiFePO_4$/C porous microspheres with a double carbon coating and found an outstanding specific discharge capacity of 120 $mAhg^{-1}$ (10 C) at 20 °C [26]. Additionally, utilizing polyvinylpyrrolidone and citric acid as complex carbon sources, Liu et al. examined $LiFePO_4$/C nanoparticles with a diameter of roughly 80 nm [27]. Due to their small size and uniformly thin carbon coating, these nanoparticles demonstrated a good discharge capacity (126 $mAhg^{-1}$) at a discharge rate of 0.1 C at 20 °C.

In addition to conductive carbon coatings, metal ion doping is often used to increase $LiFePO_4$ conductivity [28]. In order to effectively increase the low-temperature and high-rate performance of the $LiFePO_4$, Zhang et al. combined carbon aerogel coating and metal-ion doping (lanthanum- and cerium-doped $LiFePO_4$/C) [29]. Co-precipitation was used by Yang et al. to create a $LiMn_{0.8}Fe_{0.2}PO_4$/C cathode. In this way, both improved rates and low-temperature capabilities could be obtained [30]. Nano- $LiMn_{0.8}Fe_{0.2}PO_4$/C supplied 97 $mAhg^{-1}$ at 0.1 C – even at low temperatures (15 °C). $LiFePO_4$/C-Sn exhibited excellent electrochemical performance across a wide range of operating temperatures, particularly at low temperatures, when Lin et al. coated Sn nanoparticles on the surface of $LiFePO_4$ [31]. It appears that all prior studies of the $LiFePO_4$ low-temperature performance consistently showed that its reversible capacity and rate capability could be significantly reduced during operation at low temperatures.

Electric vehicles are generally more energy-efficient than conventional gasoline vehicles since they are entirely powered by lithium-ion batteries, and no exhaust emission occurs [32]. Increasing the driving range and enhancing lithium-ion battery longevity are two primary development goals for electric cars. The energy density of lithium-ion batteries directly affects their longevity, and their endurance increases with increasing energy density. In addition, enhancing the energy density of lithium-ion batteries can be done in several ways [33]. The injection volume of the entire battery can be reduced by increasing the difference between the positive electrode and negative electrode's median voltages, the positive electrode's gram capacity, the negative electrode's gram capacity, and the positive electrode's gram capacity [34, 35]. These techniques mainly enhance the positive electrode material's inherent qualities. If the positive electrode materials are identical types and the lithium-ion battery's overall weight and positive electrode volume are fixed, the energy density can be increased by increasing the positive electrode material's proportion rather than its overall volume [36]. Furthermore, reduced capacitance during fast charge and discharge can be due to very high resistance, inadequate adhesion, and a decreased ratio of conductive carbon to binder [37]. Presently, cathode materials constitute 70% of the materials used in academic research. Thus, the percentage of

Preprints (www.preprints.org) | NOT PEER-REVIEWED | Posted: 22 September 2023 doi:10.20944/preprints202309.1494.v1

LFP was increased in this study to 88%, and the electrochemical performance and mechanical stability were taken into account using the best active carbon material balance ratio.

2. Results and Discussion

FE-SEM images of Super P conductive carbon at different magnifications are shown in Figure 1(a-d). Super P appears granular, and stacking occurs. This characteristic of Super P can facilitate the filling of the positive electrode material's particles. To develop positive LFP electrode materials with the optimal amount of conductive additive and binder, the mother powder was supplemented with varying quantities of Super P conductive carbon material as an additive.

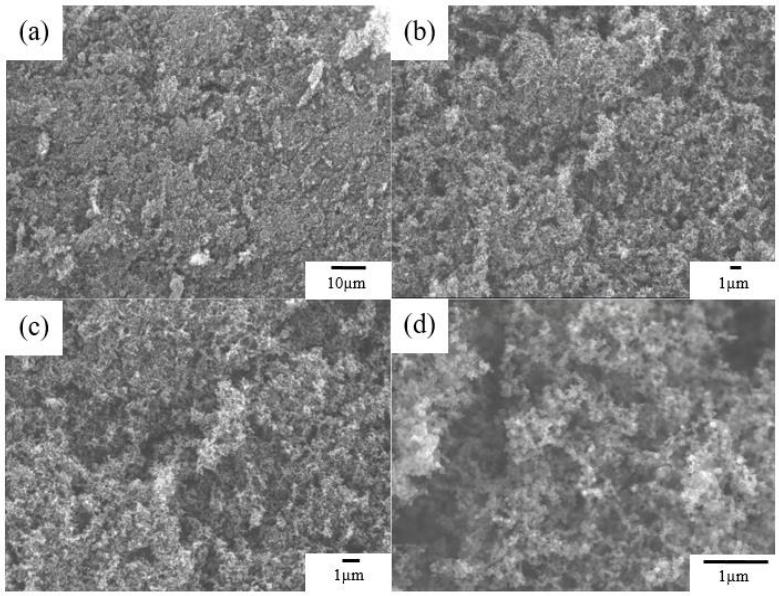

Figure 1. FE-SEM micrograph of Super P with different magnifications of (a) x1000, (b) x3000, (c) x5000, and (d) x20000.

The adhesion force measurement was carried out with an adhesion tester (MIT-AT12). To obtain samples for the adhesion test, we cut out 100 tiny squares of the surface of a positive $LiFePO_4$ electrode sheet made with different Super P ratios. The cutting speeds were 20 to 50 mm/s in the horizontal and vertical directions. To evaluate the adherence of $LiFePO_4$ cathode coating, any burrs were removed with a soft brush, and the sample was attached to the grid's surface with a special test tape. The peeling of the surface coat was evaluated according to six different categories – see Table 1. Figure 2 (a-f) shows the adhesion test results of the SP_3%, SP_4%, SP_5%, SP_5.5%, SP_6%, and SP_7% samples. The SP_3% sample showed the strongest adhesion, with only small pieces peeling off at the incision's intersection. On the other hand, the SP_7% samples showed large pieces that peeled off at the edges of the squares, which suggests the weakest adhesion. The adhesion steadily declines as the amount of conductive carbon material increases (and the amount of binder decreases). Table 2 shows the adhesion grade for all samples. AC impedance analysis is one of the most complex techniques in electrochemical research. It is an AC test technique where a sine wave signal with a specific amplitude, but variable frequency is applied to the electrochemical system to receive current feedback. The charge transfer resistances and Li^+ ion diffusion coefficients of $LiFePO_4$ cathode material samples were determined in this study via a Bio Logic VSP-300's EIS impedance analysis.

Preprints (www.preprints.org) | NOT PEER-REVIEWED | Posted: 22 September 2023 doi:10.20944/preprints202309.1494.v1

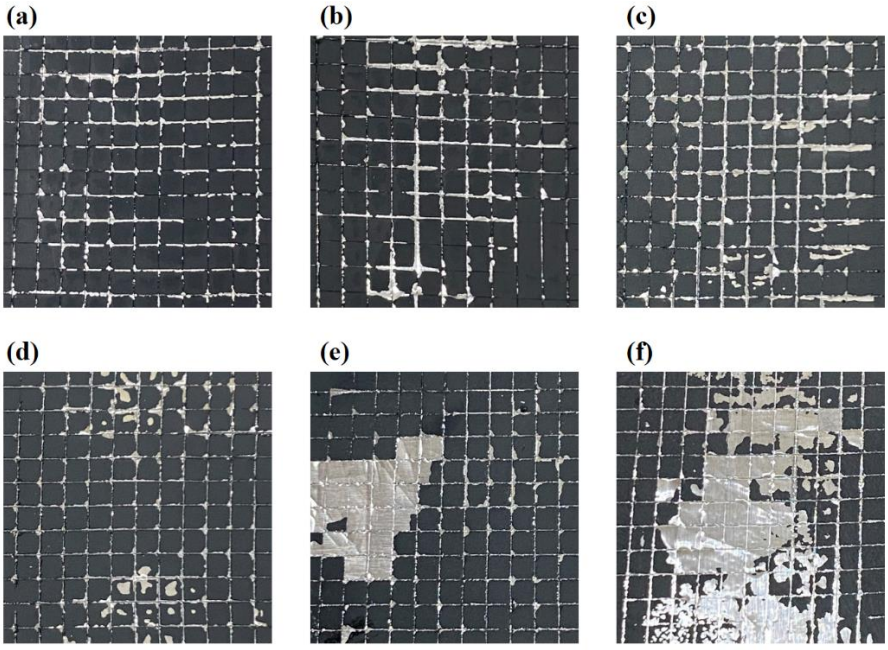

Figure 2. Adhesive force measurement of (a) SP_3%, (b) SP_4%, (c) SP_5%, (d) SP_5.5%, (e) SP_6%, and (f) SP_7% samples.

Table 1. Adhesion test standards.

ISO level	ASTM grade	Test results
0	5B	The edge of the incision is completely smooth, and the edge of the grid is not peeled off.
1	4B	There are small pieces peeling off at the intersection of the cuts, and the actual damage in the scribed area shall not exceed 5%.
2	3B	The edges and/or intersections of the incisions are peeled off, with an area of more than 5% but less than 15%.
3	2B	Partially chipped or completely chipped along the edge of the notch, and partially chipped the area was stripped more than 15%, but less than 35%.
4	1B	The edge of the cut is flaking or/or partly squared or partially peeled off, and the area

Preprints (www.preprints.org) | NOT PEER-REVIEWED | Posted: 22 September 2023 doi:10.20944/preprints202309.1494.v1

5	0B	is larger than the mark 35% of grid area, but not more than 65%. Beyond the previous level.

Table 2. Adhesion test result rating for SP_3%, SP_4%, SP_5%, SP_5.5%, SP_6%, and SP_7% samples.

Sample	ISO level	ASTM grade
SP_3%	1	4B
SP_4%	2	3B
SP_5%	2	3B
SP_5.5%	2	3B
SP_6%	4	1B
SP_7%	5	0B

The curve features two distinct segments: a high-frequency semicircle and a low-frequency oblique straight line. These represent the charge-transfer process and the diffusion resistance of the Li^+ ion in the electrochemical reaction, respectively, when the electrode reaction is controlled by both charge transfer and Li^+ ion diffusion [38]. Here the Randles equivalent circuit [39] was used as a fitting model, and EIS was used to simulate the Li^+ diffusion process. R_e denotes the combined resistance of the electrolyte and electrode material, also known as the solution resistance. This value is indicated by the high-frequency region's semicircle intercept. The charge transfer resistance of the positive electrode/electrolyte interface, represented by R_{ct}, is the diameter of the semicircle. Z_w is the reaction-diffusion process's Warburg impedance, which corresponds to the oblique line in the low-frequency region, from which the Li^+ ion diffusion coefficient can be calculated. The resulting AC impedance curves are shown in Figure 3. It can also be plotted as a function of $\omega^{-1/2}$ (ω is the angular frequency, $\omega = 2\pi f$) using the real impedance (Z'), which is shown in Figure 4. The slope σ (Equation 1) [40] is obtained from the linear fit of Z' to $\omega^{-1/2}$ from Figure 4, and the value of the slope is substituted in Equation (2) [41] to calculate the Li^+ ion diffusion coefficient (D_{EIS}) of the battery.

$$Z' = R_e + R_{ct} + \sigma\,\omega^{-1/2} \quad (1)$$

$$D_{EIS} = R^2T^2/2A^2n^4F^4C^2\sigma^2 \quad (2)$$

where, R: gas constant (J K^{-1} mol^{-1}), T: working temperature (K), A: Pole piece area (cm^2), n: number of electrons transferred, F: Faraday's constant (C mol^{-1}), C: Concentration of lithium ions in the cathode material (mole cm^{-3}).

Preprints (www.preprints.org) | NOT PEER-REVIEWED | Posted: 22 September 2023 doi:10.20944/preprints202309.1494.v1

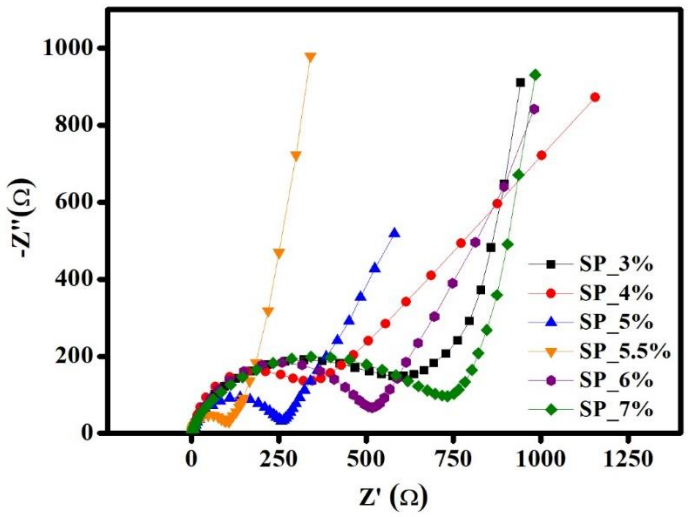

Figure 3. AC impedance spectra of SP_3%, SP_4%, SP_5%, SP_5.5%, SP_6%, and SP_7% samples at OCV.

Table 3 shows the results of the impedance simulation and the resulting Li^+ ion diffusion coefficient. Based on these findings, SP_5.5% has the lowest charge-transfer resistance (67 Ω) and the highest Li^+ ion diffusion coefficient, whereas SP_4% has the highest electrode resistance (9.97 Ω) and the lowest Li^+ ion diffusion coefficient. SP_5.5% has a lower Re than all other samples, and the sample battery has a higher Re before the discharge test. This suggests that the diffusion resistance of Li^+ ions between solutions is higher. Additionally, it has been shown that the sample's charge-transfer resistance first increases before it decreases as the amount of conductive carbon increases. The trend remains unchanged despite an order of magnitude divergence from the Li^+ ion diffusion coefficient determined based on CV. Hence, the ideal fractions for $LiFePO_4$, Super P, and PVDF are $LiFePO_4$ = 88%, Super P = 5.5%, and PVDF = 6.5%.

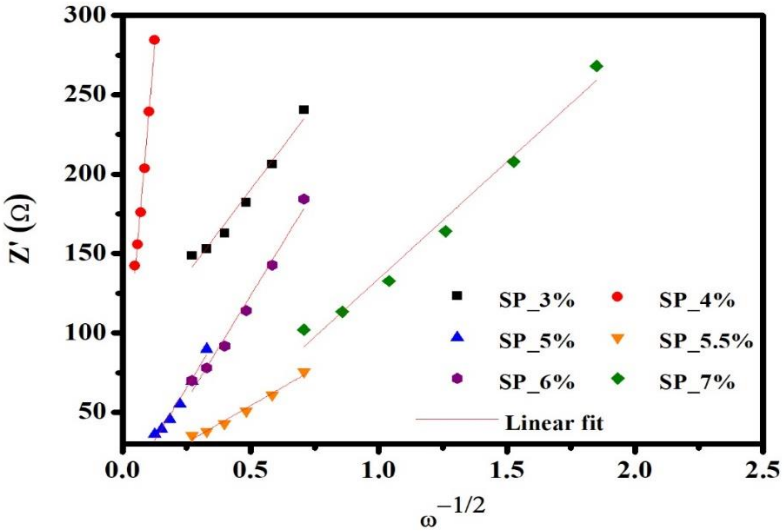

Figure 4. The relationship between Z′ and $\omega^{-1/2}$ at low frequencies of SP_3%, SP_4%, SP_5%, SP_5.5%, SP_6%, and SP_7% samples at OCV.

Table 3. The impedance parameters of SP_3%, SP_4%, SP_5%, SP_5.5%, SP_6%, and SP_7% samples at OCV.

Preprints (www.preprints.org) | NOT PEER-REVIEWED | Posted: 22 September 2023 doi:10.20944/preprints202309.1494.v1

Sample	R_e (Ω)	R_{ct} (Ω)	D_{EIS} ($cm^2 s^{-1}$)
SP_3%	2.33	338	1.08×10^{-14}
SP_4%	9.97	284	1.45×10^{-16}
SP_5%	2.71	199	6.99×10^{-15}
SP_5.5%	1.87	67	5.76×10^{-14}
SP_6%	2.26	372	7.13×10^{-15}
SP_7%	2.13	412	2.89×10^{-14}

The redox behavior of materials throughout the charging/discharging process was examined using cyclic voltammetry. To determine the relationship between voltage and current, testing involved fixing the scan cut-off voltage range, setting a certain scan rate, and repeated scanning. Here, six different scan rates (0.1, 0.2, 0.25, 0.5, 0.75, and 1 mV s^{-1}) were chosen, with the cut-off voltage varying from 2.8 to 4.0 V. The oxidation of the samples can be seen in Figure 5. The figure shows the CV curves for the SP_3%, SP_4%, SP_5%, SP_5.5%, SP_6%, and SP_7% samples and a scan rate of 0.1 mV s^{-1}. The most symmetrical and sharply decreasing peak indicates the highest electrochemical reversibility as well as the easiest intercalation and deintercalation of Li^+ ions for the given ratio. The redox findings of the samples SP_3%, SP_4%, SP_5%, SP_5.5%, SP_6% and SP_7% at various scan rates are shown in Figure 6(a-f). Furthermore, the peak currents associated with the oxidation and reduction peaks increase with the scan rate. The voltage difference (ΔV) between the redox peaks also widens gradually, which reflects the polarization of the positive electrode. It also increases and changes to higher potential and lower potentials, respectively. The smaller ΔV is, the less pronounced is the polarization. Table 4 shows the ΔV values for every sample at different scan speeds. SP_5.5% has the smallest ΔV (representing intercalation/deintercalation of Li^+ ions into LFP) among all scan rates – as well as excellent reversibility. In addition, SP_5.5% also shows the lowest polarization, the best kinetic performance, and the best electrochemical reversibility.

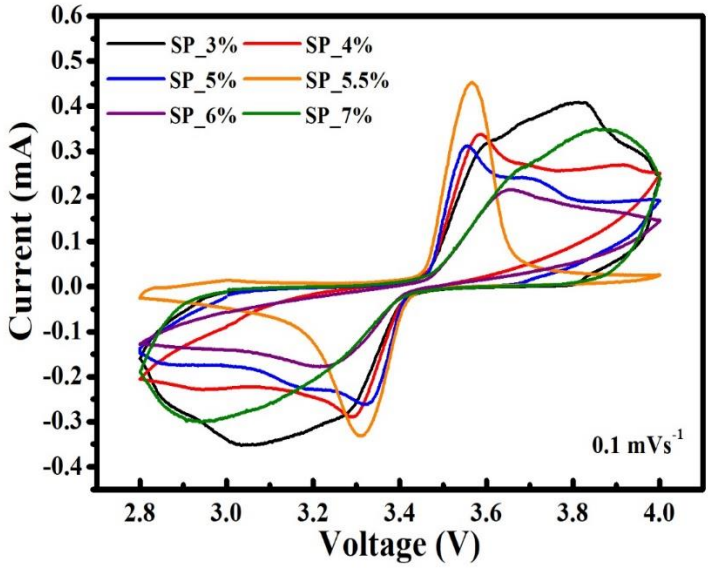

Figure 5. Cyclic voltammetry profiles of SP_3%, SP_4%, SP_5%, SP_5.5%, SP_6%, and SP_7% samples with scanning rate of 0.1 mVs^{-1} between 2.8~4.0V.

Preprints (www.preprints.org) | NOT PEER-REVIEWED | Posted: 22 September 2023 doi:10.20944/preprints202309.1494.v1

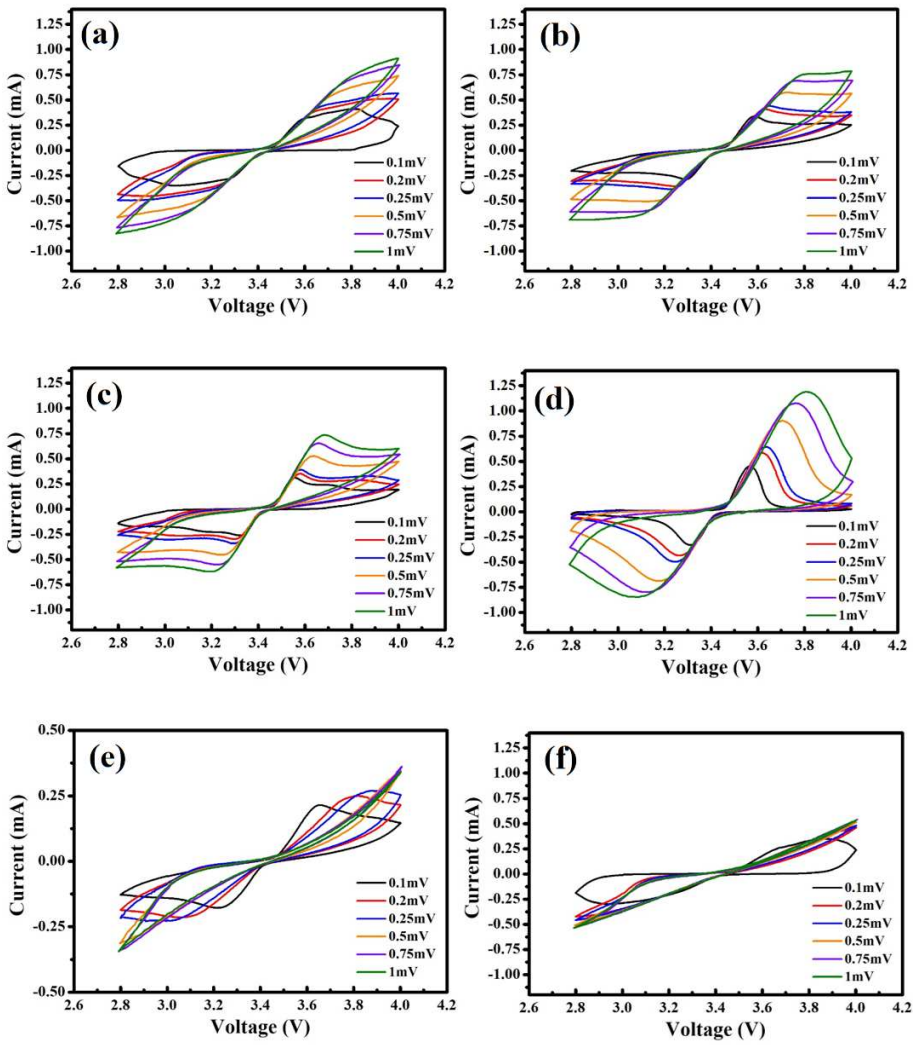

Figure 6. Cyclic voltammetry patterns of (a) SP_3%, (b) SP_4%, (c) SP_5%, (d) SP_5.5%, (e) SP_6%, and (f) SP_7% samples with the different scanning rate of 0.1 to 1 mVs^{-1} between 2.8~4.0V.

Table 4. The voltage difference (ΔV) of SP_3%, SP_4%, SP_5%, SP_5.5%, SP_6%, and SP_7% samples.

ΔV* / Scanning rate (mVs^{-1}) / Sample	0.1	0.2	0.25	0.5	0.75	1.0
SP_3%	0.77	---	---	---	---	---
SP_4%	0.30	0.39	0.42	0.60	1.00	---
SP_5%	0.26	0.35	0.39	0.54	0.64	0.73
SP_5.5%	0.23	0.28	0.29	0.39	0.43	0.49
SP_6%	0.44	0.75	0.92	---	---	---
SP_7%	0.91	---	---	---	---	---

*The ΔV is the voltage gap between maximum oxidation peak and minimum reduction peak and their voltage difference.

The peak current (I_P) was plotted as a function of the square root of the scan rate ($\nu^{1/2}$) – see Figure 7(a-d). After linear fitting, a slope ($dI/d\nu^{1/2}$) can be obtained, which is substituted into the Randles–Sevcik Equation (Equation (3)) [42], and the D_{CV} value of the diffusion coefficient for the Li^+ ions in the battery can be calculated:

Preprints (www.preprints.org) | NOT PEER-REVIEWED | Posted: 22 September 2023 doi:10.20944/preprints202309.1494.v1

$$I_P = 0.4463CS\times[(nF)^{3/2}(D_{CV}\nu)^{1/2}/(RT)^{1/2}] \quad (3)$$

where, D_{CV}: Li^+ ion diffusion coefficient ($cm^2\ s^{-1}$), I_P: Peak indicated current (A), C: Lithium ion concentration in the electrode (mole), S: pole piece area (cm^2), n: Number of electrons transferred (mol), F: Faraday's constant (96500 $C\cdot mol^{-1}$), ν: scan rate (V), R: gas constant (8.314 $J\ K^{-1}\ mol^{-1}$), T: working temperature (K).

Table 5 shows the calculated diffusion coefficients for the Li^+ ions. According to the results, the maximum diffusion coefficient ($2.6\times10^{-10}\ cm^2s^{-1}$) of the Li^+ ion was observed for SP_5.5%, and when the carbon content and the conductivity increased, the diffusion coefficient increased before it decreased.

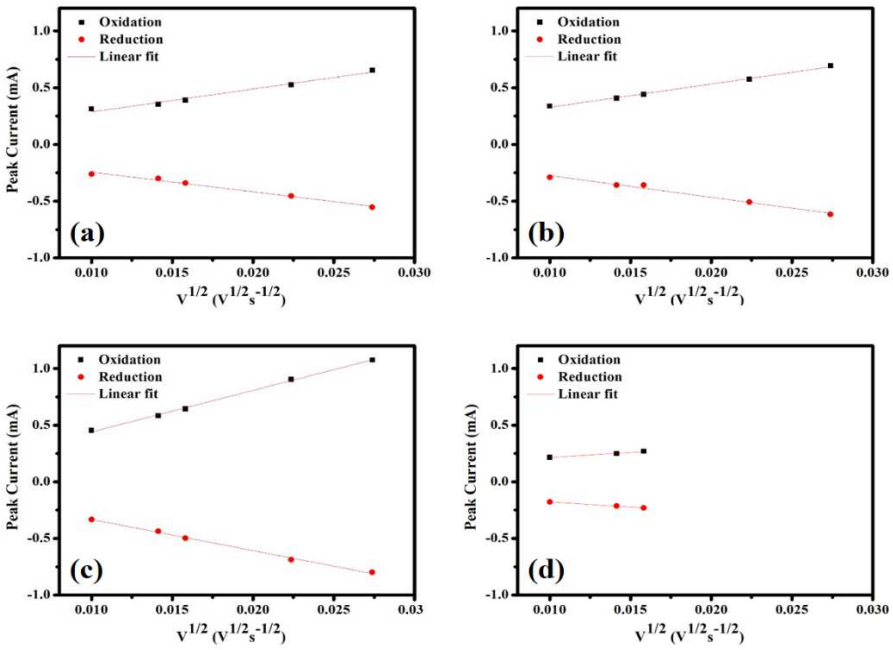

Figure 7. The relationships between peak current and the scanning rate for (a) SP_4%, (b) SP_5%, (c) SP_5.5%, and (d) SP_6% samples.

Table 5. Mechanical properties of hybrid electrolytes with various content of LiTFSI.

Sample	Tensile strength (MPa)	Elongation (%)
LiTFSI-40%	4.42	394.8
LiTFSI-50%	3.34	293.1
LiTFSI-60%	2.06	263.4
LiTFSI-70%	0.32	60.89

Lithium served as the negative electrode in the battery, while $LiFePO_4$ with different quantities of conductive carbon was used as the positive electrode, with 1M $LiPF_6$ and EC/EMC/DMC=1:1:1+1vol% VC as the electrolyte. The battery was placed in the Jiayou Technology BAT-750B charge/discharge apparatus and subjected to four distinct charge/discharge rates—0.1C (600 min), 0.5C (120 min), 1C (60 min), 5C (12 min), and 10C (6 min)—at room temperature. Each sample had a cut-off voltage range of 2.8-4.0 V. The charge/discharge curves for the samples SP_3%, SP_4%, SP_5%, SP_5.5%, SP_6% and SP_7% are shown in Figure 8(a), with a charge/discharge rate of 0.1C. The discharge capacities of SP_3%, SP_4%, SP_5%, SP_5.5%, SP_6% and SP_7% were 135.1 $mAhg^{-1}$, 152.2 $mAhg^{-1}$, 152.9 $mAhg^{-1}$, 169.8 $mAhg^{-1}$, 139.2 $mAhg^{-1}$ and 129.2 $mAhg^{-1}$, respectively. SP_5.5% had the highest discharge capacity as well as the highest charge/discharge window. The intercalation and deintercalation of Li^+ ions during the charge/discharge process are the basis of the

Preprints (www.preprints.org) | NOT PEER-REVIEWED | Posted: 22 September 2023 doi:10.20944/preprints202309.1494.v1

charge/discharge platform. In other words, this ratio improves Li^+ diffusion during the charge/discharge process and increases the discharge capacity.

Furthermore, as the conductive carbon content increases, the sample's discharge capacity increases, peaking at 6 % carbon. Subsequently, the capacity starts to decline due to insufficient binder presence. Taking into account the adhesion test results, this behavior is likely due to a weak bond between the particles and the Al substrate. Figure 8(b) displays the charge/discharge curves of each sample at different charge/discharge rates. The rates range from low to high, and the discharge capacity of every sample shows different degrees of decline. Notably, only SP_5.5% can successfully manage a 5C high-rate charge/discharge. After four different charge/discharge rate tests and returning to 0.1C, the discharge capacity was 166.5 $mAhg^{-1}$ with a retention of 98%. These numbers indicate that, for this ratio, the structure did not collapse even following a high-rate charge/discharge, and the battery remained stable.

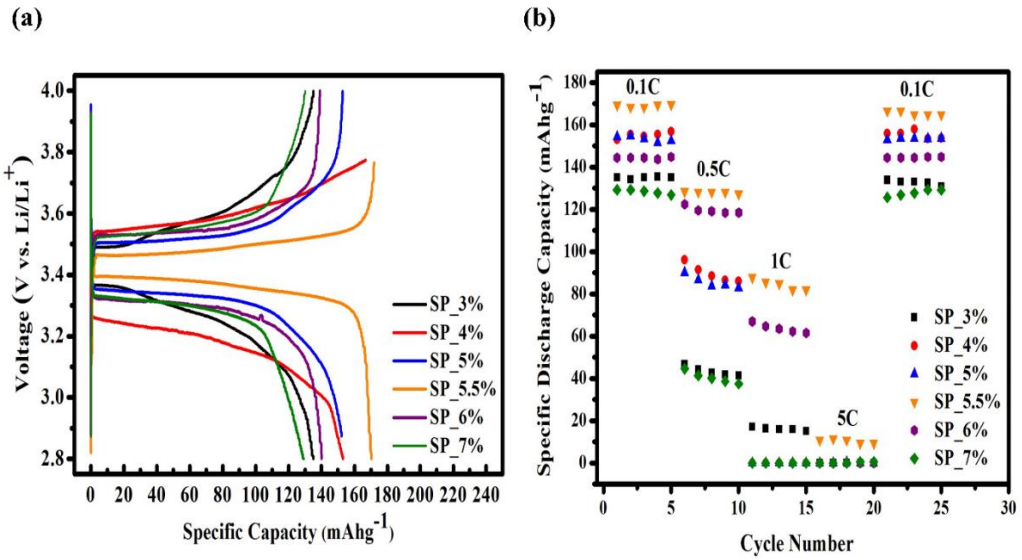

Figure 8. Electrochemical performance of SP_3%, SP_4%, SP_5%, SP_5.5%, SP_6%, and SP_7% samples between 2.8 and 4.0V. (a) Initial charge/discharge curve at 0.1C and (b) rate capacity at different current density.

3. Materials and Methods

In this work, the positive electrode sample was prepared using $LiFePO_4$, Super P (99%, Taiwan Libo) and poly (vinylidene fluoride), PVDF (99%, Jingming Chemical), which were mixed in the solvent N-methyl pyrrolidone, NMP, (99%, Jingming Chemical) with different weight ratios. The amount of Super P varied (3%, 4%, 5%, 5.5%, 6%, and 7%) to study the effect on the electrochemical properties. The used sample ratios are shown in Table 6. Firstly, PVDF was added to NMP, centrifuged, and kept for 1 h so that the powder was dissolved completely. Then, $LiFePO_4$ powder was added with different amounts of Super P, centrifuged, and kept again for 1 h to form a slurry after mixing. The slurry was evenly applied to the aluminum foil using the doctor blade method with a 200μm squeegee. The sample was then subjected to a vacuum at 100°C for 48 h to remove residual solvent, resulting in the preparation of the $LiFePO_4$ cathode sheet. In addition to the super P content, the coating thickness is very important to improve the homogeneity of the Li-ion flux. Therefore, we controlled the coating thickness by adjusting the viscosity of the slurry and the withdrawal speed during the doctor-blade coating process. Specifically, we prepared slurries with different viscosities by varying the NMP solvent content and adjusting the coating speed to obtain the desired coating thickness. We also used a micrometer to measure the thickness to ensure consistency and accuracy. Furthermore, the sheet was rolled and cut into small discs with a diameter of 13 mm to complete the production of the positive electrode. The vacuum-dried cathode piece was then cut into a small disc with a diameter of 13 mm for use in a standard R2032 coin cell. The coin cells were assembled inside

Preprints (www.preprints.org) | NOT PEER-REVIEWED | Posted: 22 September 2023 doi:10.20944/preprints202309.1494.v1

a glove box in an argon atmosphere with lithium as the anode and 1 mol $LiPF_6$ + EC/EMC/DMC = 1:1:1 vol% + 1%VC electrolyte, while keeping a standardized electrolyte-to-electrode ratio of 5 μL/mg. After keeping the sample inside the same atmosphere for one day, the electrochemical performance test was carried out.

Table 6. Ratio of sample components for positive electrode preparation.

Sample name	$LiFePO_4$ (wt%)	Super P (wt%)	PVDF (wt%)
SP_3%	88	3	9
SP_4%	88	4	8
SP_5%	88	5	7
SP_5.5%	88	5.5	6.5
SP_6%	88	6	6
SP_7%	88	7	5

An electrochemical analysis and examination of the properties of the prepared cathodes were performed as follows: The particle size and morphology of Super P conductive carbon material powder were observed using field emission scanning electron microscopy (FE-SEM, JOELJSM-6701F). A laser particle size analyzer (Beckman Coulter Particle Analyzer PN A54412) was used for the dynamic light scattering (DLS) analysis. An adhesion tester (MIT-AT12) was used to evaluate the positive $LiFePO_4$ electrodes made of different amounts of conductive carbon. For the adhesive force measurement, after cutting the grid pattern and penetrating the coating, it was pasted with a special test tape according to the peeling of the coating. The adhesion of the coating to the substrate separation was evaluated and classified into six grades to assess its quality. Cyclic voltammetry was performed using a potentiostat (Jihan-5640) at different scan rates (0.1, 0.2, 0.25, 0.5, 0.75, and 1 mVs^{-1}) with the voltage range of 2.8–4.0 V. Electrochemical impedance spectroscopy (EIS) was performed using a potentiostat (VSP-300, BioLogic) at 0.01-7 MHz under open circuit voltage. The capacity and rate performance of the fabricated coin cells were evaluated using a charge/discharge cell-test instrument (Acutech Systems, BAT-750B).

4. Conclusions

The explanations above and our experimental results present some compelling conclusions. This study used alternative conductive carbon materials (Super P) inthe active material content to enhance the volumetric energy density in lithium-ion batteries. The adhesion test indicates that when the amount of Super P increased to 5.5%, the ASTM grade could still reach 3B. However, when it increased beyond 6% or 7%, adhesion started to decrease significantly, which affected the electrochemical performance. Similarly, as the amount of conductive carbon material increased (and the amount of binder decreased), the adhesion gradually decreased. Moreover, the analysis of the cyclic voltammetry data revealed that within the range of 3% to 5.5% Super P content, a reduction in polarization in LiFePO4 occurred. This reduction impacted the diffusion coefficient of Li+ ions positively, enhancing their mobility within the material. However, when the Super P content exceeded this range, the adhesion between particles decreased, which resulted in the closure of diffusion paths for Li+ ions. This led to increased polarization and reduced overall performance. The charge/discharge test determined that the initial discharge capacity of the SP_5.5% sample (at a charge/discharge rate of 0.1C) was as high as 169.8 $mAhg^{-1}$. This number is very close to the theoretical capacity of $LiFePO_4$ (170 $mAhg^{-1}$), and only the SP_5.5% sample can manage a high-rate charge/discharge of 5C. The EIS AC impedance analysis suggests that SP_5.5% has the lowest charge-transfer impedance (67 Ω) and the highest Li^+ ion diffusion coefficient (5.76 x 10^{-14} cm^2 s^{-1}). Clearly,

conductive carbon helped improve the conductivity, but adding too much led to insufficient connectivity between the conductive carbon particles, which reduced conductivity. As a result, the optimal ratio of the three ingredients was determined as follows: $LiFePO_4$ at 88%, Super P at 5.5%, and PVDF at 6.5%. This balanced composition promotes efficient diffusion of Li+ ions during the charge/discharge process. In addition, it contributes to improved performance, particularly in high-rate charging and discharging scenarios.

Author Contributions: D.M., Conceptualization, Methodology, Investigation, Data curation, Writing-original draft preparation; M.-J.C., Investigation, Data curation, Formal analysis; I.-M.H., Conceptualization, Supervision, Funding acquisition, Writing-review and editing. All authors have read and agreed to the published version of the manuscript.

Funding: Financial support for this work was provided by the National Science and Technology Council in Taiwan through grant numbers: MOST 110-2622-E-155-011.

Conflicts of Interest: The authors declare no conflicts of interest.

References

1. Deng, D. Li-ion batteries: basics, progress, and challenges, *Energy Sci. Eng.* **2015**, *3*, 385-418. https://doi.org/10.1002/ese3.95
2. Yang, K.; Liu, Z.; Chai, J.; Zheng, Y.; Fu, X.; Shen, Y.H.; Chen, J.; Liu, Z.; Shi, S. High performance polyimide-based separator for 4.5V high voltage LiCoO2 battery with superior safety, *Mater. Chem. Phys.* **2022**, *282*, 125975-125983. https://doi.org/10.1016/j.matchemphys.2022.125975
3. Mohanty, D.; Huang, P.H.; Hung, I.M. Preparation and Characterization of a LiFePO4- Lithium Salt Composite Cathode for All-Solid-State Li-Metal Batteries, *Batteries* **2023**, *9*, 236-246. https://doi.org/10.3390/batteries9040236
4. Guo, J.; Zhang, J.; Chen, C.; Lan, Y. Rapid photodegradation of methyl orange by oxalic acis assisted with cathode material of lithium ion batteries LiFePO4, *J. Taiwan Inst. Chem. Eng.* **2016**, *62*, 187-191. https://doi.org/10.1016/j.jtice.2016.02.003
5. Mohanty, D.; Lu, Z.L.; Hung, I.M. Effect of carbon coating on electrochemical properties of Li3V2(PO4)3 cathode synthesized by citric-acid gel method for lithium-ion batteries, *J. Appl. Electrochem.* **2023**, *53*, 1003-1013. https://doi.org/10.1007/s10800-022-01828-1
6. Yang, C.C.; Jang, J.H.; Jiang, J.R. Preparation of carbon and oxide co-modified LiFePO4 cathode material for high performance lithium-ion battery, *Mater. Chem. Phys.* **2015**, *165*, 196-206. https://doi.org/10.1016/j.matchemphys.2015.09.018
7. Kraytsberg, A.; Ein-Eli, Y. Higher, Stronger, Better… A Review of 5 Volt Cathode Materials for Advanced Lithium-Ion Batteries, *Adv. Energy Mater.* **2012**, *2*, 922-939. https://doi.org/10.1002/aenm.201200068
8. Liu, H.; Liu, Y.; An, L.; Zhao, X.; Wang, L.; Liang, G. High Energy Density LiFePO4/C Cathode Material Synthesized by Wet Ball Milling Combined with Spray Drying Method, *J. Electrochem. Soc.* **2017**, *164*, A3666-A3672. DOI 10.1149/2.0011714jes
9. Nie, Z.; Liu, Y.; Yang, L.; Li, S.; Pan, F. Construction and Application of Materials Knowledge Graph Based on Author Disambiguation: Revisiting the Evolution of LiFePO4, *Adv. Energy Mater.* **2021**, *11*, 2003580-2003584. https://doi.org/10.1002/aenm.202003580
10. Cramer, C.L.; Lonescu, E.; Zajac, M.G.; Nelson, A.T.; Katoh, Y.; Haslam, J.J.; Wondraczek, L.; Aguirre, T.G.; LeBlanc, S.; Wang, H.; Masoudi, M.; Tegeler, E.; Riedel, R.; Colombo, P.; Jolandan, M.M. Additive manufacturing of ceramic materials for energy applications: Road map and opportunities, *J. Eur. Ceram. Soc.* **2022**, *42*, 3049-3088. https://doi.org/10.1016/j.jeurceramsoc.2022.01.058
11. Zhang, F.; Qi, L. Recent Progress in Self-Supported Metal Oxide Nanoarray Electrodes for Advanced Lithium-Ion Batteries, *Adv. Sci.* **2016**, *3*, 1600049-1600077. https://doi.org/10.1002/advs.201600049
12. Tang, X.C.; Li, L.X.; Lai, Q.L.; Song, X.W.; Jiang, L.H. Investigation on diffusion behavior of Li+ in LiFePO4 by capacity intermittent titration technique (CITT), *Electrochim. Acta* **2009**, *54*, 2329-2334. https://doi.org/10.1016/j.electacta.2008.10.065
13. Gao, C.; Zhou, J.; Liu, G.; Wang, L. Lithium-ions diffusion kinetic in LiFePO4/carbon nanoparticles synthesized by microwave plasma chemical vapor deposition for lithium-ion batteries, *App. Surf. Sci.* **2018**, *433*, 35-44. https://doi.org/10.1016/j.apsusc.2017.10.034
14. Chang, W.; Kim, S.J.; Park, I.T.; Cho, B.W.; Chung, K.Y.; Shin, H.C. Low temperature performance of LiFePO4 cathode material for Li-ion batteries, *J. Alloys Compd.* **2013**, *563*, 249-253. https://doi.org/10.1016/j.jallcom.2013.02.143
15. Shu, H.; Chen, M.; Fu, Y.; Yang, X.; Yi, X.; Bai, Y.; Liang, Q.; Wei, Q.; Hu, B.; Tan, J.; Zhou, M.; Wang, X. Improvement of electrochemical performance for spherical LiFePO4 via hybrid coated with electron

conductive carbon and fast Li ion conductive La0.56Li0.33TiO3, *J. Power Sources* **2014**, *252*, 73-78. https://doi.org/10.1016/j.jpowsour.2013.11.036
16. Wang, K.X.; Li, X.H.; Chen, J.S. Surface and Interface Engineering of Electrode Materials for Lithium-Ion Batteries, *Adv. Mater.* **2015**, *27*, 527-545. https://doi.org/10.1002/adma.201402962
17. Sangeeta, Agnihotri, S.; Arya, A.; Sharma, A.L. Improved electrochemical performance of the Cr doped cathode materials for energy storage/conversion devices, *AIP Conf. Proc.* **2016**, *1728*, 020380 1-5. https://doi.org/10.1063/1.4946431
18. Yao, J.; Wu, F.; Qiu, X.; Li, N.; Su, Y. Effect of CeO2-coating on the electrochemical performances of LiFePO4/C cathode material, *Electrochim. Acta* **2011**, *56*, 5587-5592. https://doi.org/10.1016/j.electacta.2011.03.141
19. Weiss, M.; Ruess, R.; Kasnatcheew, J.; Levartovsky, Y.; Lexy, N.R.; Minnmann, P.; Stolz, L.; Waldmann, T.; Mehrens, M.; Aurbach, D.; Winter, M.; Ein-Eli, Y.; Janek, J. Fast Charging of Lithium-Ion Batteries: A Review of Materials Aspects, *Adv. Energy Mater.* **2021**, *11*, 2101126-2101162. https://doi.org/10.1002/aenm.202101126
20. Weng, J.; Peng, L. Improving the electrochemical performance of LiFePO4 cathode with novel water-soluble binders, *Mater. Chem. Phys.* **2022**, *290*, 126530-126534. https://doi.org/10.1016/j.matchemphys.2022.126530
21. Örnek, A.; Bulut, E.; Özacar, M. The chemical, physical and electrochemical effects of carbon sources on the nano-scale LiFePO4 cathode surface, *Ceram. Int.* **2014**, *40*, 15727-15736. https://doi.org/10.1016/j.ceramint.2014.07.096
22. Miao, C.; Bai, P.; Jiang, Q.; Sun, S.; Wang, X. A novel synthesis and characterization of LiFePO4 and LiFePO4/C as a cathode material for lithium-ion battery, *J. Power Sources* **2014**, *246*, 232-238. https://doi.org/10.1016/j.jpowsour.2013.07.077
23. Lin, Y.; Gao, M.X.; Zhu, D.; Liu, Y.F.; Pan, H.G. Effects of carbon coating and iron phosphides on the electrochemical properties of LiFePO4/C, *J. Power Sources* **2008**, *184*, 444-448. https://doi.org/10.1016/j.jpowsour.2008.03.026
24. Zhao, N.; Li, Y.; Zhao, X.; Zhi, X.; Liang, G. Effect of particle size and purity on the low temperature electrochemical performance of LiFePO4/C cathode material, *J. Alloys Compd.* **2016**, *683*, 123-132. https://doi.org/10.1016/j.jallcom.2016.04.070
25. Cheng, F.; Wan, W.; Tan, Z.; Huang, Y.; Zhou, H.; Chen, J.; Zhang, X. High power performance of nano-LiFePO4/C cathode material synthesized via lauric acid-assisted solid-state reaction, *Electrochim. Acta* **2011**, *56*, 2999-3005. https://doi.org/10.1016/j.electacta.2011.01.007
26. Yang, C.C.; Hung, Y.W.; Lue, S.J. The Carbon Additive Effect on Electrochemical Performance of LiFe0.5Mn0.5PO4/C Composites by a Simple Solid-State Method for Lithium Ion Batteries, *Batteries* **2016**, *2*, 18-29. https://doi.org/10.3390/batteries2020018
27. Liu, H.; Miao, C.; Meng, Y.; He, Y.B.; Xu, Q.; Zhang, X.; Tang, Z. Optimized synthesis of nano-sized LiFePO4/C particles with excellent rate capability for lithium ion batteries, *Electrochim. Acta* **2014**, *130*, 322-328. https://doi.org/10.1016/j.electacta.2014.03.034
28. Eftekhari, A. LiFePO4/C nanocomposites for lithium-ion batteries, *J. Power Sources* **2017**, *343*, 395-411. https://doi.org/10.1016/j.jpowsour.2017.01.080
29. Zhang, B.; Xu, Y.; Wang, J.; Lin, J.; Wang, C.; Chen, Y, Lanthanum and cerium Co-doped LiFePO4: Morphology, electrochemical performance and kinetic study from −30 - +50 °C, *Electrochim. Acta* **2019**, *322*, 134686-134695. https://doi.org/10.1016/j.electacta.2019.134686
30. Yang, W.; Bi, Y.; Qin, Y.; Liu, Y.; Zhang, X.; Yang, B.; Wu, Q.; Wang, D.; Shi, S. LiMn0.8Fe0.2PO4/C cathode material synthesized via co-precipitation method with superior high-rate and low-temperature performances for lithium-ion batteries, *J. Power Sources* **2015**, *275*, 785-791. https://doi.org/10.1016/j.jpowsour.2014.11.063
31. Lin, Y.; Lin, Y.; Zhou, T.; Zhao, G.; Huang, Y.; Huang, Z. Enhanced electrochemical performances of LiFePO4/C by surface modification with Sn nanoparticles, *J. Power Sources* **2013**, *226*, 20-26. https://doi.org/10.1016/j.jpowsour.2012.10.074
32. Jiang, Q.; Zhang, H.; Ren, Z.; Ma, H.; Xue, M. Recent progresses of metal-organic framework-based materials in electrochemical energy storage, *Mater. Today Sustain.* **2022**, *19*, 100174-100205. https://doi.org/10.1016/j.mtsust.2022.100174